ARTICLE

doi:10.1038/nature11981

Dynamic regulatory network controlling T_H17 cell differentiation

Nir Yosef[1,2]*, Alex K. Shalek[3]*, Jellert T. Gaublomme[3]*, Hulin Jin[2], Youjin Lee[2], Amit Awasthi[2]†, Chuan Wu[2], Katarzyna Karwacz[2], Sheng Xiao[2], Marsela Jorgolli[3], David Gennert[1], Rahul Satija[1], Arvind Shakya[4], Diana Y. Lu[1], John J. Trombetta[1], Meenu R. Pillai[5], Peter J. Ratcliffe[6], Mathew L. Coleman[6], Mark Bix[5], Dean Tantin[4], Hongkun Park[1,3], Vijay K. Kuchroo[1,2] & Aviv Regev[1,7]

Despite their importance, the molecular circuits that control the differentiation of naive T cells remain largely unknown. Recent studies that reconstructed regulatory networks in mammalian cells have focused on short-term responses and relied on perturbation-based approaches that cannot be readily applied to primary T cells. Here we combine transcriptional profiling at high temporal resolution, novel computational algorithms, and innovative nanowire-based perturbation tools to systematically derive and experimentally validate a model of the dynamic regulatory network that controls the differentiation of mouse T_H17 cells, a proinflammatory T-cell subset that has been implicated in the pathogenesis of multiple autoimmune diseases. The T_H17 transcriptional network consists of two self-reinforcing, but mutually antagonistic, modules, with 12 novel regulators, the coupled action of which may be essential for maintaining the balance between T_H17 and other $CD4^+$ T-cell subsets. Our study identifies and validates 39 regulatory factors, embeds them within a comprehensive temporal network and reveals its organizational principles; it also highlights novel drug targets for controlling T_H17 cell differentiation.

Effective coordination of the immune system requires careful balancing of distinct pro-inflammatory and regulatory $CD4^+$ helper T-cell populations. Among those, pro-inflammatory IL-17 producing T_H17 cells have a key role in the defence against extracellular pathogens and have also been implicated in the induction of several autoimmune diseases[1]. T_H17 differentiation from naive T cells can be triggered *in vitro* by the cytokines TGF-β1 and IL-6. Whereas TGF-β1 alone induces $Foxp3^+$ regulatory T cells (T_{reg} cells)[2], the presence of IL-6 inhibits T_{reg} development and induces T_H17 differentiation[1].

Much remains unknown about the regulatory network that controls the differentiation of T_H17 cells[3,4]. Developmentally, as TGF-β is required for both T_H17 and induced T_{reg} differentiation, it is not fully understood how balance is achieved between them or how IL-6 produces a bias towards T_H17 differentiation[1]. Functionally, it is unclear how the pro-inflammatory status of T_H17 cells is held in check by the immunosuppressive cytokine IL-10 (refs 3, 4). Finally, many of the key regulators and interactions that drive the development of T_H17 cells remain unknown[5].

Recent studies have demonstrated the power of coupling systematic profiling with perturbation for deciphering mammalian regulatory circuits[6–9]. Most of these studies have relied upon computational circuit-reconstruction algorithms that assume one 'fixed' network. T_H17 differentiation, however, spans several days, during which the components and wiring of the regulatory network probably change. Furthermore, naive T cells and T_H17 cells cannot be transfected effectively *in vitro* by traditional methods without changing their phenotype or function, thus limiting the effectiveness of perturbation strategies for inhibiting gene expression.

Here we address these limitations by combining transcriptional profiling, novel computational methods and nanowire-based short interfering RNA (siRNA) delivery[10] (Fig. 1a) to construct and validate the transcriptional network of T_H17 differentiation. The reconstructed model is organized into two coupled, antagonistic and densely intra-connected modules, one promoting and the other suppressing the T_H17 program. The model highlights 12 novel regulators, the function of which we further characterized by their effects on global gene expression, DNA binding profiles, or T_H17 differentiation in knockout mice.

A transcriptional time course of T_H17 differentiation

We induced the differentiation of naive $CD4^+$ T cells into T_H17 cells using TGF-β1 and IL-6, and measured transcriptional profiles using microarrays at 18 time points along a 72-h time course (Fig. 1, Supplementary Fig. 1a–c and Methods). As controls, we measured mRNA profiles for cells that were activated without the addition of differentiating cytokines (T_H0). We identified 1,291 genes that were differentially expressed specifically during T_H17 differentiation (Methods and Supplementary Table 1) and partitioned them into 20 co-expression clusters (*k*-means clustering; Methods, Fig. 1b and Supplementary Fig. 2) with distinct temporal profiles. We used these clusters to characterize the response and reconstruct a regulatory network model, as described below (Fig. 2a).

Three main waves of transcription and differentiation

There are three transcriptional phases as the cells transition from a naive-like state ($t = 0.5$ h) to T_H17 ($t = 72$ h; Fig. 1c and Supplementary Fig. 1c): early (up to 4 h), intermediate (4–20 h), and late (20–72 h). Each corresponds, respectively, to a differentiation phase[5]: (1) induction; (2) onset of phenotype and amplification; and (3) stabilization and IL-23 signalling. The early phase is characterized

[1]Broad Institute of MIT and Harvard, 7 Cambridge Center, Cambridge, Massachusetts 02142, USA. [2]Center for Neurologic Diseases, Brigham & Women's Hospital, Harvard Medical School, Boston, Massachusetts 02115, USA. [3]Department of Chemistry and Chemical Biology and Department of Physics, Harvard University, Cambridge, Massachusetts 02138, USA. [4]Department of Pathology, University of Utah School of Medicine, Salt Lake City, Utah 84132, USA. [5]Department of Immunology, St. Jude Children's Research Hospital, Memphis, Tennessee 38105, USA. [6]University of Oxford, Headington Campus, Oxford OX3 7BN, UK. [7]Howard Hughes Medical Institute, Department of Biology, Massachusetts Institute of Technology, Cambridge, Massachusetts 02140, USA. †Present address: Translational Health Science & Technology Institute, Faridabad, Haryana 122016, India.
*These authors contributed equally to this work.

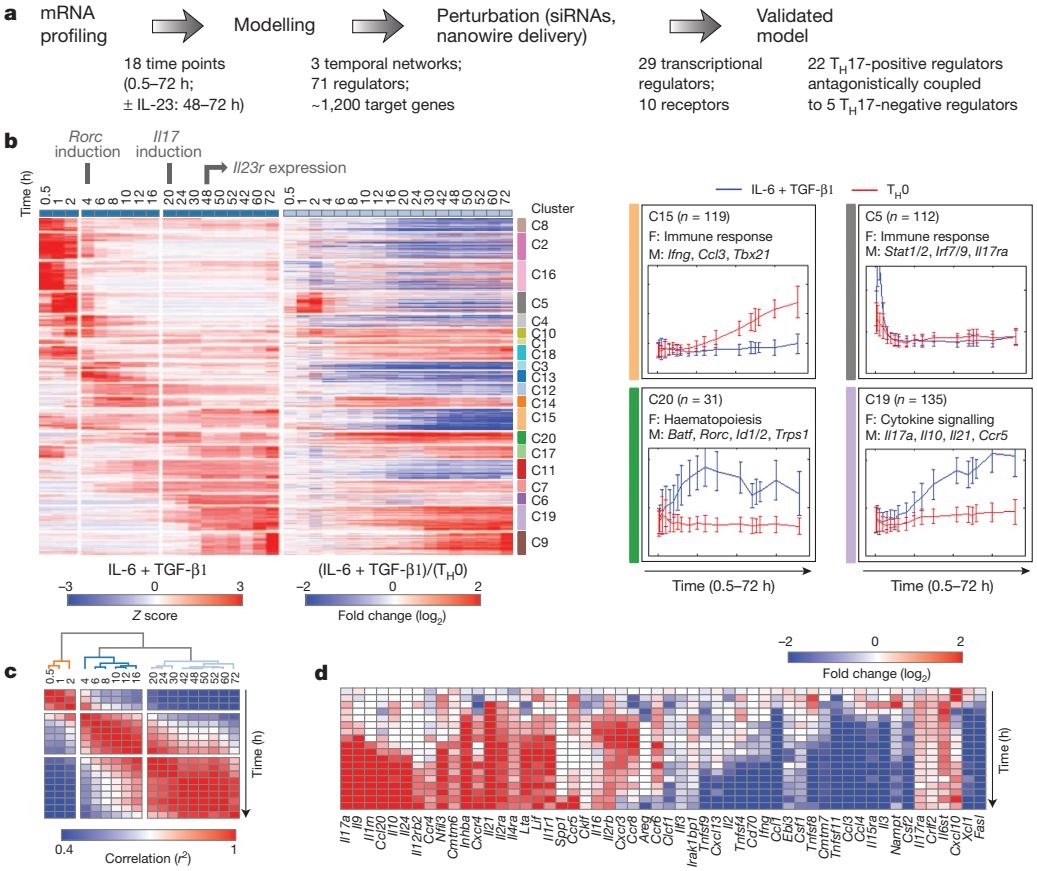

Figure 1 | Genome-wide temporal expression profiles of T_H17 differentiation. **a**, Overview of approach. **b**, Gene expression profiles during T_H17 differentiation. Shown are the differential expression levels for genes (rows) at 18 time points (columns) in T_H17 polarizing conditions (TGF-β1 and IL-6; left panel, *Z*-normalized per row) or T_H17 polarizing conditions relative to control activated T_H0 cells (right panel, $\log_2$(ratio)). The genes are partitioned into 20 clusters (C1–C20, colour bars, right). Right: mean expression (*y* axis) and standard deviation (error bar) at each time point (*x* axis) for genes in representative clusters. Cluster size (*n*), enriched functional annotations (F) and representative genes (M) are denoted. **c**, Three major transcriptional phases. Shown is a correlation matrix (red, high; blue, low) between every pair of time points. **d**, Transcriptional profiles of key cytokines, chemokines and their receptors. Time points are the same as in panel **b**.

by transient induction (for example, cluster C5, Fig. 1b) of immune response pathways (for example, IL-6 and TGF-β signalling; Supplementary Table 2). Some early induced genes display sustained expression (for example, cluster C10, Fig. 1b); these are enriched for transcription factors, including the key T_H17 factors *Stat3*, *Irf4* and *Batf*, and the cytokine and cytokine receptors *Il21*, *Lif* and *Il2ra* (Supplementary Table 1). The transition to the intermediate phase ($t = 4$ h) is marked by induction of the *Rorc* gene (encoding the master transcription factor ROR-γt; Supplementary Fig. 1d) and another 12 transcription factors (cluster C20, Fig. 1b), both known (for example, *Ahr*) and novel (for example, *Trps1*) in T_H17 differentiation. During the transition to the late phase ($t = 20$ h), mRNAs of T_H17 signature cytokines are induced (for example, *Il17a*, *Il9*; cluster C19) whereas mRNAs of cytokines that signal other T-cell lineages are repressed (for example, *Ifng* and *Il4*). Regulatory cytokines from the IL-10 family are also induced (*Il10*, *Il24*), possibly as a self-limiting mechanism related to the emergence of 'pathogenic' or 'non-pathogenic' T_H17 cells[11]. Around 48 h, the cells induce *Il23r* (data not shown), which has an important role in the late phase (Supplementary Fig. 3 and Supplementary Table 1).

Inference of dynamic regulatory interactions

We proposed the hypothesis that each of the clusters (Fig. 1b and Supplementary Table 2) encompasses genes that share regulators active in the relevant time points. To predict these regulators, we assembled a general network of regulator–target associations from published genomics profiles[12–19] (Fig. 2a and Methods). We then connected a regulator to a gene from its set of putative targets only if there was also a significant overlap between the regulator's putative targets and that gene's cluster (Methods). Because different regulators act at different times, the connection between a regulator and its target may be active only within a certain time window. To determine this window, we labelled each edge with a time stamp denoting when both the target gene is regulated (based on its expression profile) and the regulator node is expressed at sufficient levels (based on its mRNA levels and inferred protein levels[20]; Methods). In this way, we derived a network 'snapshot' for each of the 18 time points (Fig. 2b–d). Overall, 10,112 interactions between 71 regulators and 1,283 genes were inferred in at least one network.

Substantial regulatory re-wiring during differentiation

The active factors and interactions change from one network to the next. The vast majority of interactions are active only at some time windows (Fig. 2c), even for regulators (for example, Batf) that participate in all networks. On the basis of similarity in active interactions, we identified three network classes (Fig. 2c) corresponding to the three differentiation phases (Fig. 2d). We collapsed all networks in each phase into one model, resulting in three consecutive network models (Fig. 2d, Supplementary Fig. 4 and Supplementary Table 3). Among the regulators, 33 are active in all of the networks (for example, known master regulators such as Batf, Irf4 and Stat3), whereas 18 are active primarily in one (for example, Stat1 and Irf1 in the early network; ROR-γt in the late network). Indeed, whereas *Rorc* mRNA levels are induced at ~4 h, ROR-γt protein levels increase

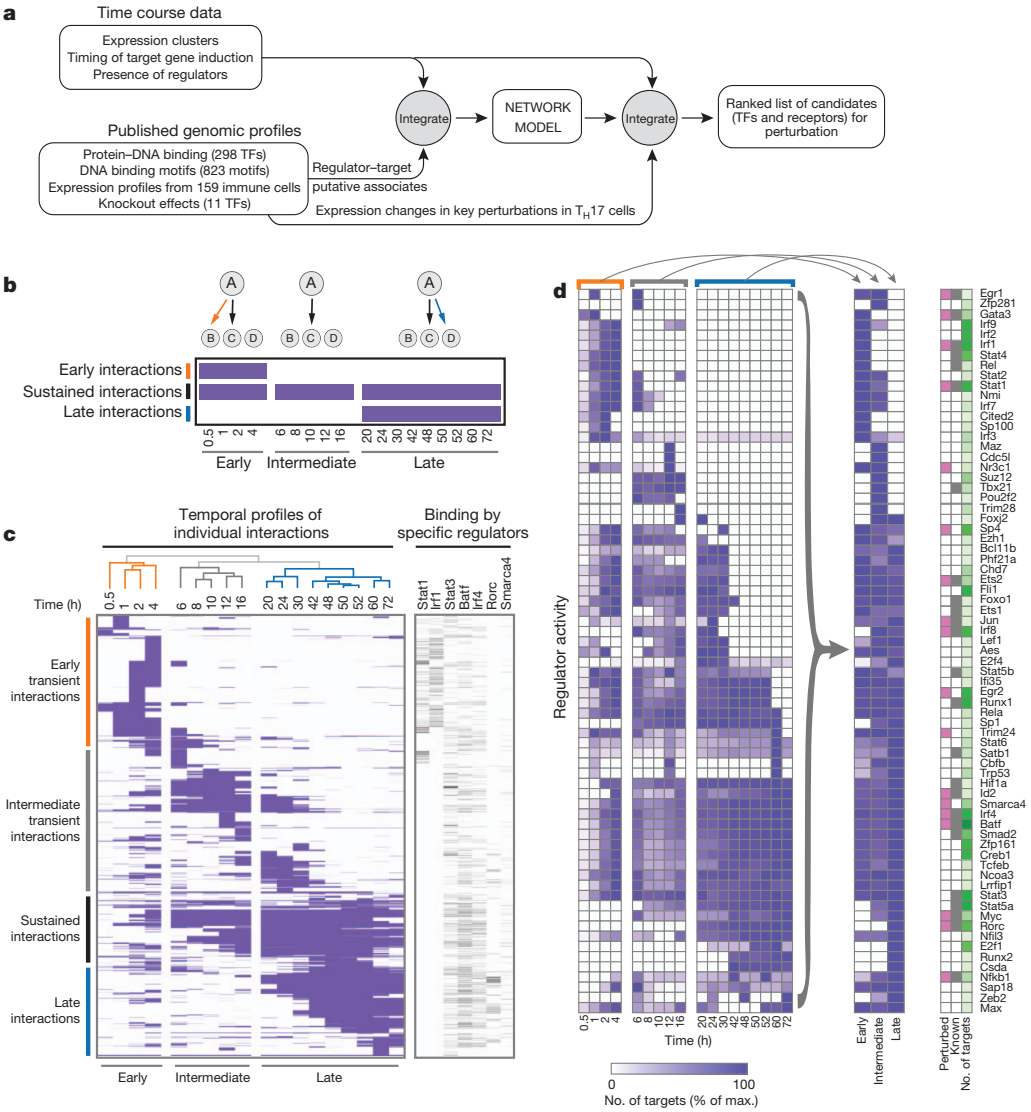

Figure 2 | A model of the dynamic regulatory network of T_H17 differentiation. **a**, Overview of computational analysis. **b**, Schematic of temporal network 'snapshots'. Shown are three consecutive cartoon networks (top and matrix columns), with three possible interactions from regulator (A) to targets (B, C and D), shown as edges (top) and matrix rows (A→B, top row; A→C, middle row; A→D, bottom row). **c**, Eighteen network 'snapshots'. Left: each row corresponds to a transcription factor (TF)–target interaction that occurs in at least one network; columns correspond to the network at each time point. A purple entry an indicates that an interaction is active in that network. The networks are clustered by similarity of active interactions (dendrogram, top), forming three temporally consecutive clusters (early, intermediate, late; bottom). Right: heat map denoting edges for selected regulators. **d**, Dynamic regulator activity. Shown is, for each regulator (rows), the number of target genes (normalized by its maximum number of targets) in each of the 18 networks (columns, left), and in each of the three canonical networks (middle) obtained by collapsing (arrows). Right: regulators chosen for perturbation (pink), known T_H17 regulators (grey), and the maximal number of target genes across the three canonical networks (green, ranging from 0 to 250 targets).

at approximately 20 h and further rise over time, consistent with our model (Supplementary Fig. 5).

Ranking novel regulators for systematic perturbation

In addition to known T_H17 regulators, our network includes dozens of novel factors as predicted regulators (Fig. 2d), induced target genes, or both (Supplementary Fig. 4 and Supplementary Table 3). It also contains receptor genes as induced targets, both previously known in T_H17 cells (for example, *Il1r1*, *Il17ra*) and novel (for example, *Fas*, *Itga3*).

We ranked candidate regulators for perturbation (Figs 2a and 3a; see Methods), guided by features that reflect a regulatory role (Fig. 3a, 'Network information') and a role as a target (Fig. 3a, 'Gene expression information'). We computationally ordered the genes to emphasize certain features (for example, a predicted regulator of key T_H17 genes) over others (for example, differential expression in our time course data). We used a similar scheme to rank receptor proteins (Supplementary Table 4 and Methods). Supporting their quality, our top-ranked factors are enriched ($P < 10^{-3}$) for manually curated T_H17 regulators (Supplementary Fig. 6), and correlate well (Spearman $r > 0.86$) with a ranking learned by a supervised method (Methods). We chose 65 genes for perturbation: 52 regulators and 13 receptors (Supplementary Table 4). These included most of the top 44 regulators and top 9 receptors (excluding a few well known T_H17 genes and/or those for which knockout data already existed), as well as additional representative lower ranking factors.

Nanowire-based perturbation of primary T cells

In unstimulated primary mouse T cells, viral- or transfection-based siRNA delivery has been nearly impossible because it either alters differentiation or cell viability[21,22]. We therefore used a new delivery technology based on silicon nanowires[10,23], which we optimized to deliver siRNA effectively (>95%) into naive T cells without activating them (Fig. 3b, c)[23].

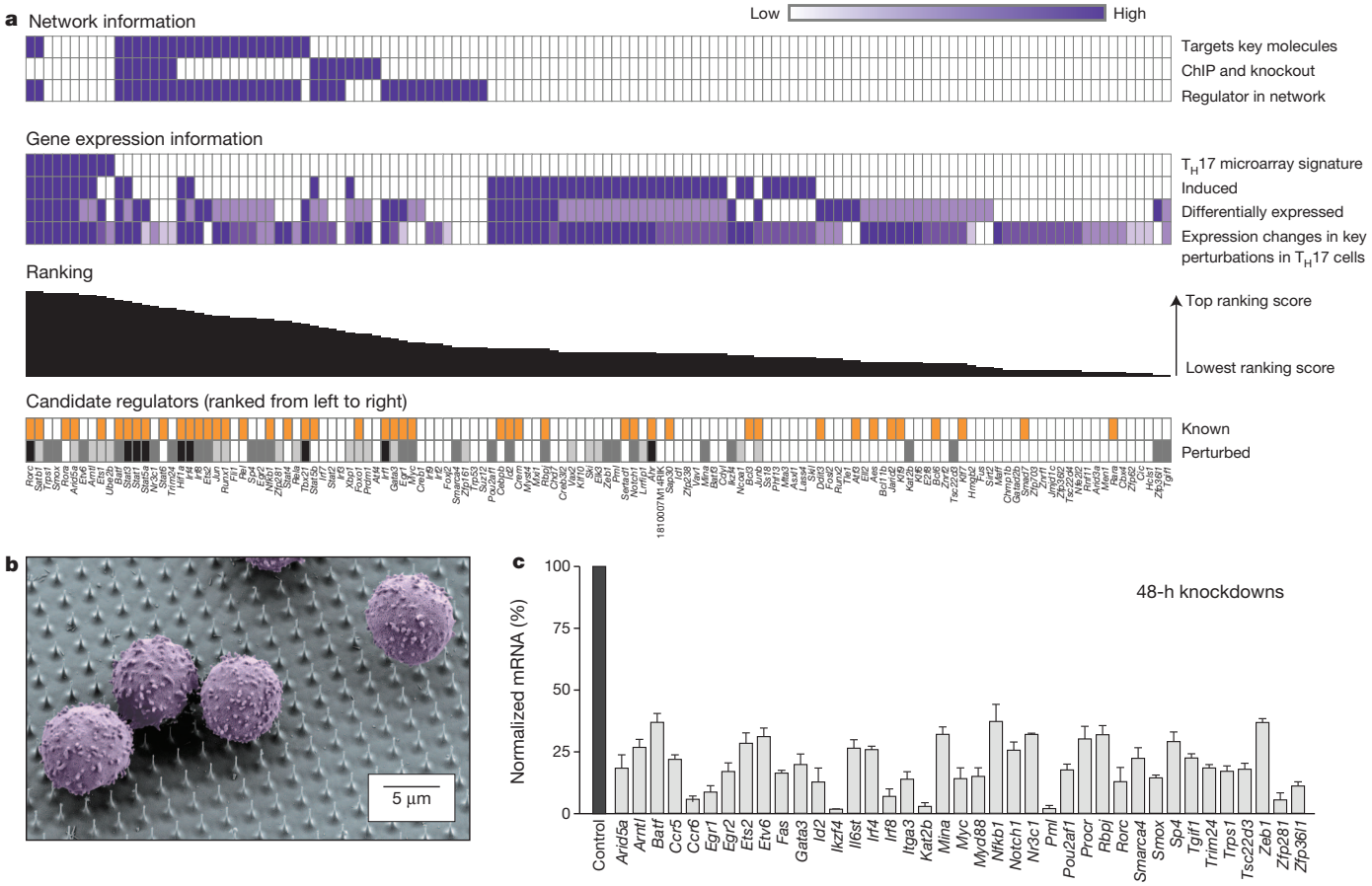

Figure 3 | Knockdown screen in T_H17 differentiation using silicon nanowires. **a**, Unbiased ranking of perturbation candidates. Shown are the genes ordered from left to right based on their ranking for perturbation (columns, top ranking is left-most). Two top matrices: criteria for ranking by 'Network information' (topmost) and 'Gene expression information'. Purple entry: gene has the feature (intensity proportional to feature strength; top five features are binary). Bar chart indicates ranking score. 'Perturbed' row: dark grey, genes successfully perturbed by knockdown followed by high-quality mRNA quantification; light grey, genes that we attempted to knockdown but could not achieve or maintain sufficient knockdown or did not obtain enough replicates; Black, genes that we perturbed by knockout or for which knockout data were already available. Known row: orange entry: a gene was previously associated with T_H17 function (this information was not used to rank the genes; Supplementary Fig. 6). **b**, Scanning electron micrograph of primary T cells (false-coloured purple) cultured on vertical silicon nanowires. **c**, Effective knockdown by siRNA delivered on nanowires. Shown is the percentage of mRNA remaining after knockdown (by qPCR, *y* axis: mean ± standard error relative to non-targeting siRNA control, $n = 12$, black bar on left) at 48 h after activation.

We attempted to perturb 60 genes with nanowire-mediated siRNA delivery and achieved efficient knockdown (<60% transcript remaining at 48 h post-activation) for 34 genes (Fig. 3c and Supplementary Fig. 7). We obtained knockout mice for seven other genes, two of which (*Irf8* and *Il17ra*) were also in the knockdown set (Supplementary Table 4). Altogether, we successfully perturbed 39 of the 65 selected genes—29 regulators and 10 receptors—including 21 genes not previously associated with T_H17 differentiation.

Nanowire-based screen validates 39 network regulators

We measured the effects of perturbations at 48 h post-activation on the expression of 275 signature genes using the Nanostring nCounter system (Supplementary Tables 5 and 6; *Il17ra* and *Il21r* knockouts were also measured at 60 h). The signature genes were computationally chosen to cover as many aspects of the differentiation process as possible (Methods): they include most differentially expressed cytokines, transcription factors, and cell-surface molecules, as well as representatives from each cluster (Fig. 1b) or enriched function (Supplementary Table 2), and predicted targets in each network (Supplementary Table 3). For validation, we profiled a signature of 86 genes using the Fluidigm BioMark system, obtaining highly reproducible results (Supplementary Fig. 8).

We scored the statistical significance of a perturbation's effect on a signature gene by comparing to non-targeting siRNAs and to 18 control genes that were not differentially expressed (Supplementary Information and Fig. 4a, all non-grey entries are significant). Supporting the original network model (Fig. 2), there is a significant overlap between the genes affected by a regulator's knockdown and its predicted targets ($P \leq 0.01$, permutation test; Supplementary Information).

To study the network's dynamics, we measured the effect of 28 of the perturbations at 10 h (shortly after the induction of *Rorc*; Supplementary Table 5) using the Fluidigm BioMark system. We found that 30% of the functional interactions are present with the same activation/repression logic at both 10 h and 48 h, whereas the rest are present only in one time point (Supplementary Fig. 9). This is consistent with the extent of rewiring in our original model (Fig. 2c).

Two coupled antagonistic circuits in the T_H17 network

Characterizing each regulator by its effect on T_H17 signature genes (for example, *Il17a*, *Il17f*; Fig. 4b, grey nodes, bottom), we found that, at 48 h, the network is organized into two antagonistic modules: a module of 22 'T_H17-positive factors' (Fig. 4b, blue nodes: 9 novel), the perturbation of which decreased the expression of T_H17 signature genes (Fig. 4b, grey nodes, bottom), and a module of 5 'T_H17-negative factors' (Fig. 4b, red nodes: 3 novel), the perturbation of which had the opposite effect. Each of the modules is tightly intra-connected through positive, self-reinforcing interactions between its members

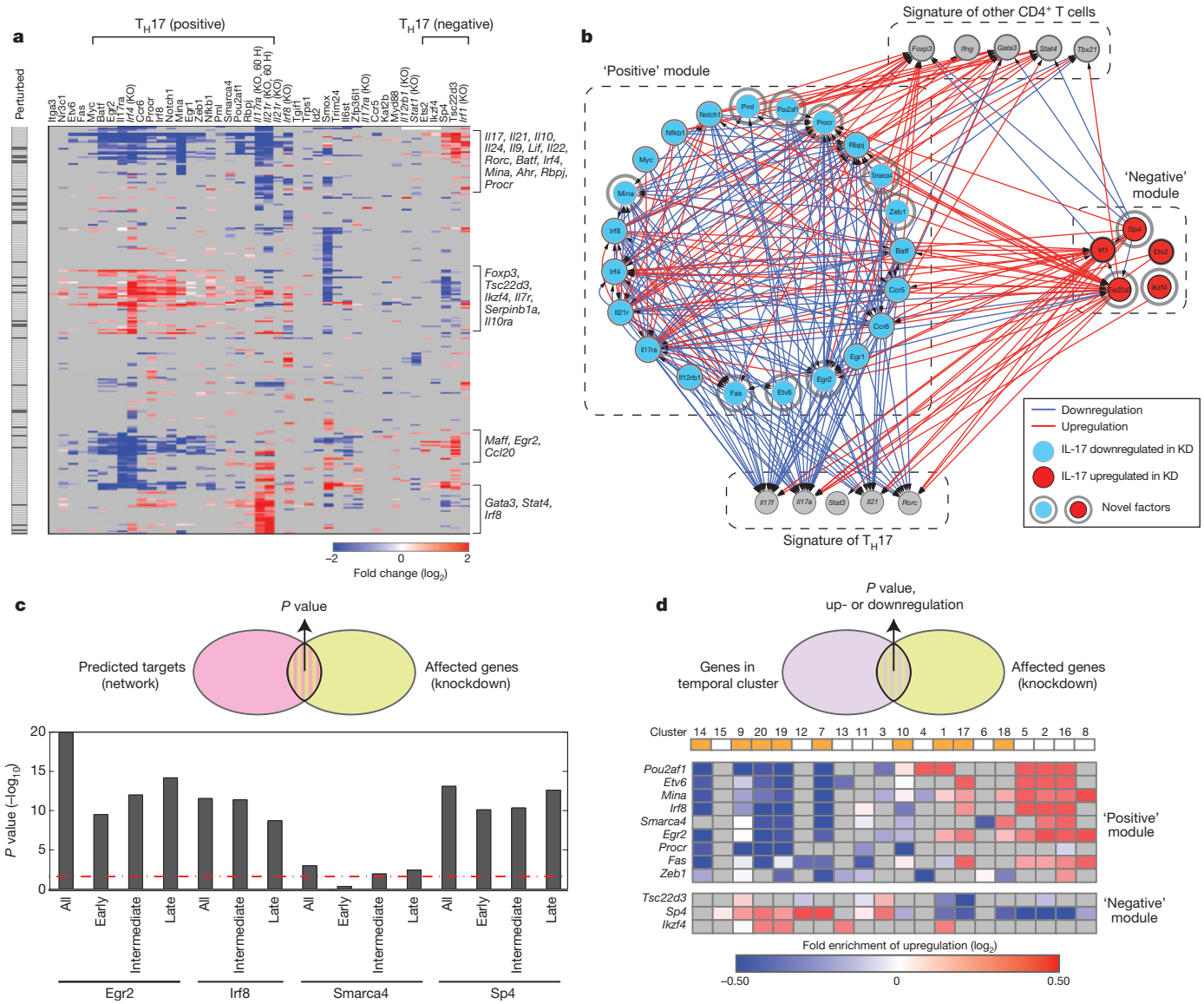

Figure 4 | Coupled and mutually antagonistic modules in the T_H17 network. **a**, Impact of perturbed genes on a 275-gene signature. Shown are changes in the expression of 275 signature genes (rows) following knockdown or knockout (KO) of 39 factors (columns) at 48 h (as well as *Il21r* and *Il17ra* knockout at 60 h). Blue, decreased expression of target following perturbation of a regulator (compared to a non-targeting control); red, increased expression; grey, not significant; all non-grey entries are significant (Supplementary Information). Perturbed (left): signature genes that are also perturbed as regulators (black entries). Key signature genes are denoted on right. **b**, Two coupled and opposing modules. Shown is the perturbation network associating the 'positive regulators' (blue nodes) of T_H17 signature genes, the 'negative regulators' (red nodes), T_H17 signature genes (grey nodes, bottom) and signature genes of other $CD4^+$ T cells (grey nodes, top). A blue edge from node A to B indicates that knockdown of A downregulates B; a red edge indicates that knockdown of A upregulates B. Light-grey halos: regulators not previously associated with T_H17 differentiation. **c**, Knockdown effects validate edges in network model. Venn diagram: we compare the set of targets for a factor in the original model of Fig. 2a (pink circle) to the set of genes that respond to that factor's knockdown in an RNA-seq experiment (yellow circle). Bar chart (bottom): shown is the $-\log_{10}$(*P* value) (*y* axis, hypergeometric test) for the significance of this overlap for four factors (*x* axis). Similar results were obtained with a non-parametric rank-sum test (Mann–Whitney *U*-test, Supplementary Information). Red dashed line: $P = 0.01$. **d**, Global knockdown effects are consistent across clusters. Venn diagram: we compare the set of genes that respond to a factor's knockdown in an RNA-seq experiment (yellow circle) to each of the 20 clusters of Fig. 1b (purple circle). We expect the knockdown of a 'T_H17 positive' regulator to repress genes in induced clusters, and induce genes in repressed clusters (and vice versa for 'T_H17 negative' regulators). Heat map: for each regulator knockdown (rows) and each cluster (columns) shown are the significant overlaps (non-grey entries) by the test above. Red, fold enrichment for upregulation upon knockdown; blue, fold enrichment for downregulation upon knockdown. Orange entries in the top row indicate induced clusters.

(70% of the intra-module edges), whereas most (88%) inter-module interactions are negative. This organization, which is statistically significant (empirical *P* value $<10^{-3}$; Methods, Supplementary Fig. 10), is reminiscent of that observed previously in genetic circuits in yeast[24,25]. At 10 h, the same regulators do not yield this clear pattern ($P > 0.5$), suggesting that, at that point, the network is still malleable.

The two antagonistic modules may have a key role in maintaining the balance between T_H17 and other T-cell subsets and in self-limiting the pro-inflammatory status of T_H17 cells. Indeed, perturbing T_H17-positive factors also induces signature genes of other T-cell subsets, whereas perturbing T_H17-negative factors suppresses them (for example, *Foxp3*, *Gata3* and *Stat4*; Fig. 4b, grey nodes, top).

Validation and characterization of novel factors

Next, we focused on the role of 12 of the positive or negative factors (including 11 of the 12 novel factors that have not been associated with T_H17 cells; Fig. 4b, light-grey halos). After knockdown of each factor, we used RNA-seq analysis to test whether its predicted targets

(Fig. 2) were affected (Fig. 4c, Venn diagram, top). We found highly significant overlaps ($P < 10^{-5}$) for three of the factors (*Egr2*, *Irf8* and *Sp4*) that exist in both data sets, and a borderline significant overlap for the fourth (*Smarca4*), validating the quality of the edges in our network.

Next, we assessed the designation of each of the 12 factors as 'T_H17 positive' or 'T_H17 negative' by comparing the set of genes that respond to that factor's knockdown (in RNA-seq) to each of the 20 clusters (Fig. 1b). Consistent with the original definitions, knockdown of a T_H17-positive regulator downregulated genes in otherwise induced clusters and upregulated genes in otherwise repressed or uninduced clusters (and vice versa for T_H17-negative regulators; Fig. 4d and Supplementary Fig. 11a, b). The genes affected by either positive or negative regulators also significantly overlap with those bound by key $CD4^+$ transcription factors (for example, Foxp3 (refs 26, 27), Batf, Irf4 and ROR-γt (refs 28, 29), S. Xiao *et al.*, unpublished data).

Mina promotes the T_H17 and inhibits the Foxp3 program

Knockdown of Mina, a chromatin regulator from the Jumonji C (JmjC) family, represses the expression of signature T_H17 cytokines and transcription factors (for example, *Rorc*, *Batf*, *Irf4*) and of late-induced genes (clusters C9 and C19; $P < 10^{-5}$; Supplementary Tables 5 and 7), while increasing the expression of *Foxp3*, the master transcription factor of T_{reg} cells. Mina is strongly induced during T_H17 differentiation (cluster C7), is downregulated in $Il23r^{-/-}$ T_H17 cells, and is a predicted target of Batf[30], ROR-γt[30] and Myc in our model (Fig. 5a). Mina was shown to suppress T_H2 bias by interacting with the transcription factor NFAT and repressing the *Il4* promoter[31]. However, in our cells, Mina knockdown did not induce T_H2 genes, indicating an alternative mode of action via positive feedback loops between Mina, Batf and ROR-γt (Fig. 5a, left). Consistent with this model, *Mina* expression is reduced in T_H17 cells from *Rorc* knockout mice, and the *Mina* promoter was found to be bound by ROR-γt by ChIP-seq (data not shown). Finally, the genes induced by Mina knockdown significantly overlap with those bound by Foxp3 in T_{reg} cells[26,27] ($P < 10^{-25}$; Supplementary Table 7) and with a cluster previously linked to Foxp3 activity in T_{reg} cells[32] (Supplementary Fig. 11c and Supplementary Table 7).

To analyse the role of Mina further, we measured IL-17a and Foxp3 expression after differentiation of naive T cells from $Mina^{-/-}$ mice. $Mina^{-/-}$ cells had decreased IL-17a and increased $Foxp3^+$ T cells compared to wild-type cells, as detected by intracellular staining (Fig. 5a). Cytokine analysis of the corresponding supernatants confirmed a decrease in IL-17a production and an increase in IFN-γ (Fig. 5a) and TNF-α (Supplementary Fig. 12a). This is consistent with a model where Mina, induced by ROR-γt and Batf, promotes transcription of *Rorc*, while suppressing induction of *Foxp3*, thus affecting the reciprocal T_{reg}/T_H17 balance[33] by favouring rapid T_H17 differentiation.

Fas promotes the T_H17 program and suppresses IFN-γ

Fas, the TNF receptor superfamily member 6, is another T_H17-positive regulator (Fig. 5b). *Fas* is induced early and is a target of Stat3 and Batf in our model. Fas knockdown represses the expression of key T_H17 genes (for example, *Il17a*, *Il17f*, *Hif1a*, *Irf4* and *Rbpj*) and of the induced cluster C14, and promotes the expression of T_H1-related genes, including *Ifngr1* and *Klrd1* (CD94; by RNA-seq, Figs 4, 5b, Supplementary Table 7 and Supplementary Fig. 11). Fas- and Fas-ligand-deficient mice are resistant to the induction of autoimmune encephalomyelitis (EAE)[34], but have no defect in IFN-γ or T_H1 responses. The mechanism underlying this phenomenon has not been identified.

To explore this, we differentiated T cells from $Fas^{-/-}$ mice (Fig. 5b and Supplementary Fig. 12c). Consistent with our knockdown analysis, expression of IL-17a was strongly repressed and IFN-γ production was strongly increased under both T_H17 and T_H0 polarizing conditions (Fig. 5b). These results suggest that besides being a death receptor, Fas may have an important role in controlling the T_H1/T_H17 balance, and $Fas^{-/-}$ mice may be resistant to EAE due to lack of T_H17 cells.

Pou2af1 promotes the T_H17 program and suppresses IL-2 expression

Knockdown of Pou2af1 (also called OBF1) strongly decreases the expression of T_H17 signature genes (Fig. 5c) and of intermediate- and late-induced genes (clusters C19 and C20, $P < 10^{-7}$; Supplementary Tables 5 and 7), while increasing the expression of regulators of other $CD4^+$ subsets (for example, *Foxp3*, *Stat4*, *Gata3*) and of genes in

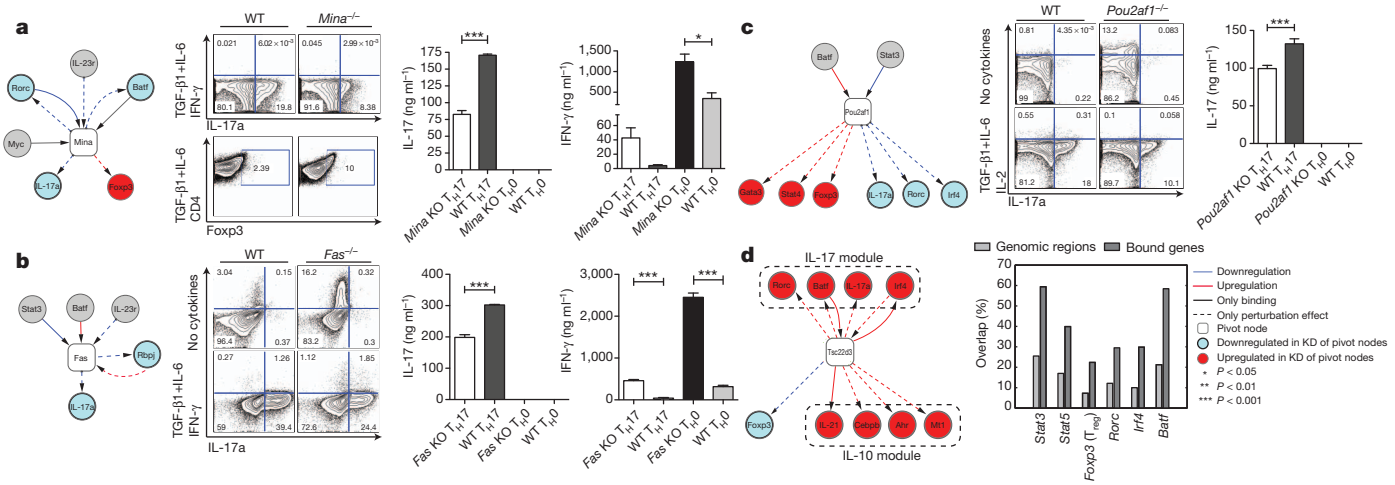

Figure 5 | Mina, Fas, Pou2af1 and Tsc22d3 are key novel regulators affecting the T_H17 differentiation programs. **a**–**d**, Left: shown are regulatory network models centred on different pivotal regulators (square nodes; **a**, Mina; **b**, Fas; **c**, Pou2af1; **d**, Tsc22d3). In each network, shown are the targets and regulators (round nodes) connected to the pivotal nodes based on perturbation (red and blue dashed edges), transcription factor binding (black solid edges), or both (red and blue solid edges). Genes affected by perturbing the pivotal nodes are coloured (blue, target is downregulated by knockdown of pivotal node; red, target is upregulated). Middle and right panels of **a**–**c**: intracellular staining and cytokine assays by ELISA or cytometric bead assays (CBA) on culture supernatants at 72 h of *in vitro* differentiated cells from respective knockout mice activated *in vitro* with anti-CD3 plus anti-CD28 with or without T_H17 polarizing cytokines (TGF-β1 plus IL-6). **d**, Middle: ChIP-seq of Tsc22d3. Shown is the proportion of overlap in bound genes (dark grey) or bound regions (light grey) between Tsc22d3 and a host of T_H17 canonical factors (*x* axis). All results are statistically significant ($P < 10^{-6}$; Hypergeometric score (gene overlap) and Binomial score (region overlap); Supplementary Information).

non-induced clusters (clusters C2 and C16, $P < 10^{-9}$; Supplementary Table 5 and 7). The role of Pou2af1 in T-cell differentiation has not been explored[35].

To investigate its effects, we differentiated T cells from *Pou2af1*$^{-/-}$ mice (Fig. 5c and Supplementary Fig. 12b). Compared to wild-type cells, IL-17a production was strongly repressed. Interestingly, IL-2 production was strongly increased in *Pou2af1*$^{-/-}$ T cells under non-polarizing (T_H0) conditions. Thus, Pou2af1 may promote T_H17 differentiation by blocking production of IL-2, a known endogenous repressor of T_H17 cells[36]. Pou2af1 acts as a transcriptional co-activator of the transcription factors Oct1 or Oct2 (ref. 35). IL-17a production was also strongly repressed in Oct1-deficient cells (Supplementary Fig. 12d), suggesting that Pou2af1 may exert some of its effects through this co-factor.

Tsc22d3 may limit T_H17 generation and inflammation

Knockdown of the TSC22 domain family protein 3 (Tsc22d3) increases the expression of T_H17 cytokines (*Il17a*, *Il21*) and transcription factors (*Rorc*, *Rbpj*, *Batf*), and reduces *Foxp3* expression. Previous studies in macrophages have shown that *Tsc22d3* expression is stimulated by glucocorticoids and IL-10, and it has a key role in their anti-inflammatory and immunosuppressive effects[37]. Tsc22d3 knockdown in T_H17 cells increased the expression of *Il10* and other key genes that enhance its production (Fig. 5d). Although IL-10 production has been shown[33,38,39] to render T_H17 cells less pathogenic in autoimmunity, co-production of IL-10 and IL-17a may be the indicated response for clearing certain infections such as *Staphylococcus aureus* at mucosal sites[40]. This suggests a model where Tsc22d3 is part of a negative feedback loop for the induction of a T_H17 cell subtype that co-produces IL-17 and IL-10 and limits their pro-inflammatory capacity. Tsc22d3 is induced in other cells in response to the steroid dexamethasone[41], which represses T_H17 differentiation and *Rorc* expression[42]. Thus, Tsc22d3 may mediate this effect of steroids.

To characterize the role of Tsc22d3 further, we used ChIP-seq to measure its DNA-binding profile in T_H17 cells and RNA-seq following its knockdown to measure its functional effects. There is a significant overlap between Tsc22d3's functional and physical targets ($P < 0.01$, for example, *Il21*, *Irf4*; Supplementary Information and Supplementary Table 8). For example, Tsc22d3 binds to *Il21* and *Irf4*, which also become upregulated in the Tsc22d3 knockdown. Furthermore, the Tsc22d3 binding sites significantly overlap those of major T_H17 factors, including Batf, Stat3, Irf4 and ROR-γt (>5-fold enrichment; Fig. 5d, Supplementary Table 8 and Supplementary Methods). This suggests a model where Tsc22d3 exerts its T_H17-negative function as a transcriptional repressor that competes with T_H17-positive regulators over binding sites, analogous to previous findings in $CD4^+$ regulation[29,43].

Discussion

We combined a high-resolution transcriptional time course, novel methods to reconstruct regulatory networks, and innovative nanotechnology to perturb T cells, to construct and validate a network model for T_H17 differentiation. The model consists of three consecutive, densely intra-connected networks, implicates 71 regulators (46 novel), and suggests substantial rewiring in 3 phases. The 71 regulators significantly overlap with genes genetically associated with inflammatory bowel disease[44] (11 of 71, $P < 10^{-9}$). Building on this model, we systematically ranked 127 putative regulators (82 novel; Supplementary Table 4) and tested top ranking ones experimentally.

We found that the T_H17 regulators are organized into two tightly coupled, self-reinforcing but mutually antagonistic modules, the coordinated action of which may explain how the balance between T_H17, T_{reg} and other effector T-cell subsets is maintained, and how progressive directional differentiation of T_H17 cells is achieved. Within the two modules are 12 novel factors (Figs 4 and 5), which we further characterized, highlighting four of the factors (others are in Supplementary Note and Supplementary Fig. 13).

A recent study[29] systematically ranked T_H17 regulators based on ChIP-seq data for known key factors and transcriptional profiles in wild-type and knockout cells. Whereas their network centred on known core T_H17 transcription factors, our complementary approach perturbed many genes in a physiologically meaningful setting. Reassuringly, their core T_H17 network significantly overlaps with our computationally inferred model (Supplementary Fig. 14).

The wiring of the positive and negative modules (Figs 4 and 5) uncovers some of the functional logic of the T_H17 program, but probably involves both direct and indirect interactions. Our functional model provides an excellent starting point for deciphering the underlying physical interactions with DNA binding profiles[30] or protein–protein interactions (accompanying paper[45]). The regulators that we identified are compelling new targets for regulating the T_H17/T_{reg} balance and for switching pathogenic T_H17 into non-pathogenic ones.

METHODS SUMMARY

We measured gene expression profiles at 18 time points (0.5 to 72 h) under T_H17 conditions (IL-6, TGF-β1) or control (T_H0) using Affymetrix microarrays HT_MG-430A. We detected differentially expressed genes using a consensus over four inference methods, and clustered the genes using *k*-means clustering, with an automatically derived *k*. Temporal regulatory interactions were inferred by looking for significant ($P < 5 \times 10^{-5}$ and fold enrichment >1.5) overlaps between the regulator's putative targets (for example, based on ChIP-seq) and the target gene's cluster (using four clustering schemes). Candidates for perturbation were ordered lexicographically using network-based and expression-based features. Perturbations were done using SiNW for siRNA delivery.

Full Methods and any associated references are available in the online version of the paper.

Received 28 September 2012; accepted 5 February 2013.
Published online 6 March 2013.

1. Bettelli, E., Oukka, M. & Kuchroo, V. K. T_H-17 cells in the circle of immunity and autoimmunity. *Nature Immunol.* **8,** 345–350 (2007).
2. Zhou, L. *et al.* TGF-β-induced Foxp3 inhibits T_H17 cell differentiation by antagonizing RORγt function. *Nature* **453,** 236–240 (2008).
3. O'Shea, J. *et al.* Signal transduction and Th17 cell differentiation. *Microbes Infect.* **11,** 599–611 (2009).
4. Zhou, L. & Littman, D. Transcriptional regulatory networks in Th17 cell differentiation. *Curr. Opin. Immunol.* **21,** 146–152 (2009).
5. Korn, T., Bettelli, E., Oukka, M. & Kuchroo, V. K. IL-17 and Th17 cells. *Annu. Rev. Immunol.* **27,** 485–517 (2009).
6. Amit, I. *et al.* Unbiased reconstruction of a mammalian transcriptional network mediating pathogen responses. *Science* **326,** 257–263 (2009).
7. Novershtern, N. *et al.* Densely interconnected transcriptional circuits control cell states in human hematopoiesis. *Cell* **144,** 296–309 (2011).
8. Litvak, V. *et al.* Function of C/EBPδ in a regulatory circuit that discriminates between transient and persistent TLR4-induced signals. *Nature Immunol.* **10,** 437–443 (2009).
9. Suzuki, H. *et al.* The transcriptional network that controls growth arrest and differentiation in a human myeloid leukemia cell line. *Nature Genet.* **41,** 553–562 (2009).
10. Shalek, A. K. *et al.* Vertical silicon nanowires as a universal platform for delivering biomolecules into living cells. *Proc. Natl Acad. Sci. USA* **107,** 1870–1875 (2010).
11. Lee, Y. *et al.* Induction and molecular signature of pathogenic T_H17 cells. *Nature Immunol.* **13,** 991–999 (2012).
12. Linhart, C., Halperin, Y. & Shamir, R. Transcription factor and microRNA motif discovery: the Amadeus platform and a compendium of metazoan target sets. *Genome Res.* **18,** 1180–1189 (2008).
13. Zheng, G. *et al.* ITFP: an integrated platform of mammalian transcription factors. *Bioinformatics* **24,** 2416–2417 (2008).
14. Wilson, N. K. *et al.* Combinatorial transcriptional control in blood stem/progenitor cells: genome-wide analysis of ten major transcriptional regulators. *Cell Stem Cell* **7,** 532–544 (2010).
15. Lachmann, A. *et al.* ChEA: transcription factor regulation inferred from integrating genome-wide ChIP-X experiments. *Bioinformatics* **26,** 2438–2444 (2010).
16. Liberzon, A. *et al.* Molecular signatures database (MSigDB) 3.0. *Bioinformatics* **27,** 1739–1740 (2011).
17. Jiang, C., Xuan, Z., Zhao, F. & Zhang, M. TRED: a transcriptional regulatory element database, new entries and other development. *Nucleic Acids Res.* **35,** D137–D140 (2007).
18. Elkon, R., Linhart, C., Sharan, R., Shamir, R. & Shiloh, Y. Genome-wide *in silico* identification of transcriptional regulators controlling the cell cycle in human cells. *Genome Res.* **13,** 773–780 (2003).

19. Heng, T. S. & Painter, M. W. The Immunological Genome Project: networks of gene expression in immune cells. *Nature Immunol.* **9,** 1091–1094 (2008).
20. Schwanhäusser, B. *et al.* Global quantification of mammalian gene expression control. *Nature* **473,** 337–342 (2011).
21. Dardalhon, V. *et al.* Lentivirus-mediated gene transfer in primary T cells is enhanced by a central DNA flap. *Gene Ther.* **8,** 190–198 (2001.
22. McManus, M. *et al.* Small interfering RNA-mediated gene silencing in T lymphocytes. *J. Immunol.* **169,** 5754 (2002).
23. Shalek, A. K. *et al.* Nanowire-mediated delivery enables functional interrogation of primary immune cells: application to the analysis of chronic lymphocytic leukemia. *Nano Lett.* **12,** 6498–6504 (2012).
24. Segrè, D., Deluna, A., Church, G. M. & Kishony, R. Modular epistasis in yeast metabolism. *Nature Genet.* **37,** 77–83 (2005).
25. Peleg, T., Yosef, N., Ruppin, E. & Sharan, R. Network-free inference of knockout effects in yeast. *PLOS Comput. Biol.* **6,** e1000635 (2010).
26. Marson, A. *et al.* Foxp3 occupancy and regulation of key target genes during T-cell stimulation. *Nature* **445,** 931–935 (2007).
27. Zheng, Y. *et al.* Genome-wide analysis of Foxp3 target genes in developing and mature regulatory T cells. *Nature* **445,** 936–940 (2007).
28. Glasmacher, E. *et al.* A genomic regulatory element that directs assembly and function of immune-specific AP-1-IRF complexes. *Science* **338,** 975–980 (2012).
29. Ciofani, M. *et al.* A validated regulatory network for Th17 cell specification. *Cell* **151,** 289–303 (2012).
30. Glasmacher, E. *et al.* A genomic regulatory element that directs assembly and function of immune-specific AP-1-IRF complexes. *Science* **338,** 975–980 (2012).
31. Okamoto, M. *et al.* Mina, an Il4 repressor, controls T helper type 2 bias. *Nature Immunol.* **10,** 872–879 (2009).
32. Hill, J. A. *et al.* Foxp3 transcription-factor-dependent and -independent regulation of the regulatory T cell transcriptional signature. *Immunity* **27,** 786–800 (2007).
33. Korn, T. *et al.* IL-21 initiates an alternative pathway to induce proinflammatory T_H17 cells. *Nature* **448,** 484–487 (2007).
34. Waldner, H., Sobel, R. A., Howard, E. & Kuchroo, V. K. Fas- and FasL-deficient mice are resistant to induction of autoimmune encephalomyelitis. *J. Immunol.* **159,** 3100–3103 (1997).
35. Teitell, M. A. OCA-B regulation of B-cell development and function. *Trends Immunol.* **24,** 546–553 (2003).
36. Laurence, A. *et al.* Interleukin-2 signaling via STAT5 constrains T helper 17 cell generation. *Immunity* **26,** 371–381 (2007).
37. Choi, S.-J. *et al.* Tsc-22 enhances TGF-β signaling by associating with Smad4 and induces erythroid cell differentiation. *Mol. Cell. Biochem.* **271,** 23–28 (2005).
38. Peters, A., Lee, Y. & Kuchroo, V. K. The many faces of Th17 cells. *Curr. Opin. Immunol.* **23,** 702–706 (2011).
39. Chaudhry, A. *et al.* Interleukin-10 signaling in regulatory T cells is required for suppression of Th17 cell-mediated inflammation. *Immunity* **34,** 566–578 (2011).
40. Zielinski, C. E. *et al.* Pathogen-induced human T_H17 cells produce IFN-γ or IL-10 and are regulated by IL-1β. *Nature* **484,** 514–518 (2012).
41. Jing, Y. *et al.* A mechanistic study on the effect of dexamethasone in moderating cell death in Chinese Hamster Ovary cell cultures. *Biotechnol. Prog.* **28,** 490–496 (2012).
42. Hu, S. M., Luo, Y. L., Lai, W. Y. & Chen, P. F. Effects of dexamethasone on intracellular expression of Th17 cytokine interleukin 17 in asthmatic mice [in Chinese]. *Nan Fang Yi Ke Da Xue Xue Bao* **29,** 1185–1188 (2009).
43. Yang, X. P. *et al.* Opposing regulation of the locus encoding IL-17 through direct, reciprocal actions of STAT3 and STAT5. *Nature Immunol.* **12,** 247–254 (2011).
44. Jostins, L. *et al.* Host–microbe interactions have shaped the genetic architecture of inflammatory bowel disease. *Nature* **491,** 119–124 (2012).
45. Wu, C. *et al.* Induction of pathogenic T_H17 cells by inducible salt-sensing kinase SGK1. *Nature* http://dx.doi.org/10.1038/nature11984 (2013).

Supplementary Information is available in the online version of the paper.

Acknowledgements We thank L. Gaffney and L. Solomon for artwork, the Broad's Genomics Platform for sequencing, and D. Kozoriz for cell sorting. Work was supported by NHGRI (1P50HG006193-01 to H.P. and A.R.), NIH Pioneer Awards (5DP1OD003893-03 to H.P., DP1OD003958-01 to A.R.), NIH (NS 30843, NS045937, AI073748 and AI45757 to V.K.K.), National MS Society (RG2571 to V.K.K.), HHMI (A.R.), and the Klarman Cell Observatory (A.R.).

Author Contributions N.Y., A.K.S., J.T.G., H.P., V.K.K. and A.R. conceived the study and designed experiments. N.Y. developed computational methods. N.Y., A.K.S. and J.T.G. analysed the data. A.K.S., J.T.G., H.J., Y.L., A.A., C.W., K.K., S.X., M.J., D.G., R.S., D.Y.L. and J.J.T. conducted the experiments. A.S., M.R.P., P.J.R., M.L.C., M.B. and D.T. provided knockout mice. N.Y., A.K.S., J.T.G., V.K.K., H.P. and A.R. wrote the paper with input from all the authors.

Author Information The microarray, RNA-seq and ChIP-seq data sets have been deposited in the Gene Expression Omnibus database under accession numbers GSE43955, GSE43969, GSE43948 and GSE43949. Reprints and permissions information is available at www.nature.com/reprints. The authors declare no competing financial interests. Readers are welcome to comment on the online version of the paper. Correspondence and requests for materials should be addressed to H.P. (Hongkun_Park@harvard.edu), V.K.K. (vkuchroo@rics.bwh.harvard.edu) or A.R. (aregev@broad.mit.edu).

METHODS

Mice. C57BL/6 wild-type, *Irf1*$^{-/-}$, *Fas*$^{-/-}$, *Irf4*$^{fl/fl}$ and *Cd4*^{Cre} mice were obtained from Jackson Laboratory. *Stat1*$^{-/-}$ and 129/Sv control mice were purchased from Taconic. *Il12rb1*$^{-/-}$ mice were provided by P. Kalipada. *Il17ra*$^{-/-}$ mice were provided by J. Kolls. *Irf8*$^{fl/fl}$ mice were provided by K. Ozato. Both *Irf4*$^{fl/fl}$ and *Irf8*$^{fl/fl}$ mice were crossed to *Cd4*^{Cre} mice to generate *Cd4*^{Cre}×*Irf4*$^{fl/fl}$ and *Cd4*^{Cre}×*Irf8*$^{fl/fl}$ mice. All animals were housed and maintained in a conventional pathogen-free facility at the Harvard Institute of Medicine in Boston (IUCAC protocols: 0311-031-14 (V.K.K.) and 0609-058015 (A.R.)). All experiments were performed in accordance to the guidelines outlined by the Harvard Medical Area Standing Committee on Animals at the Harvard Medical School. In addition, spleens from *Mina*$^{-/-}$ mice were provided by M. Bix (IACUC protocol: 453). *Pou2af1*$^{-/-}$ mice were obtained from the laboratory of R. Roeder[46]. Wild-type and *Oct1*$^{-/-}$ fetal livers were obtained at day E12.5 and transplanted into sub-lethally irradiated *Rag1*$^{-/-}$ mice as previously described[47] (IACUC protocol: 11-09003).

Cell sorting and *in vitro* T-cell differentiation. CD4^{+} T cells were purified from spleen and lymph nodes using anti-CD4 microbeads (Miltenyi Biotech) then stained in PBS with 1% FCS for 20 min at room temperature with anti-CD4-PerCP, anti-CD62l-APC and anti-CD44-PE antibodies (all Biolegend). Naive CD4^{+}CD62l^{high}CD44^{low} T cells were sorted using the BD FACSAria cell sorter. Sorted cells were activated with plate-bound anti-CD3 (2 μg ml^{-1}) and anti-CD28 (2 μg ml^{-1}) in the presence of cytokines. For T_H17 differentiation: 2 ng ml^{-1} rhTGF-β1 (Miltenyi Biotec), 25 ng ml^{-1} rmIl-6 (Miltenyi Biotec), 20 ng ml^{-1} rmIl-23 (Miltenyi Biotec), and 20 ng ml^{-1} rmIL-β1 (Miltenyi Biotec). Cells were cultured for 0.5–72 h and collected for RNA, intracellular cytokine staining, and flow cytometry.

Flow cytometry and intracellular cytokine staining. Sorted naive T cells were stimulated with phorbol 12-myristate 13-aceate (PMA) (50 ng ml^{-1}, Sigma-aldrich), ionomycin (1 μg ml^{-1}, Sigma-aldrich) and a protein transport inhibitor containing monensin (Golgistop) (BD Biosciences) for 4 h before detection by staining with antibodies. Surface markers were stained in PBS with 1% FCS for 20 min at room temperature, then subsequently the cells were fixed in Cytoperm/Cytofix (BD Biosciences), permeabilized with Perm/Wash Buffer (BD Biosciences) and stained with Biolegend conjugated antibodies, that is, Brilliant violet 650 anti-mouse IFN-γ (XMG1.2) and allophycocyanin-anti-IL-17A (TC11-18H10.1), diluted in Perm/Wash buffer as described[48] (Fig. 5 and Supplementary Fig. 11). To measure the time course of ROR-γt protein expression, a phycoerythrin-conjugated anti- retinoid-related orphan receptor-γ was used (B2D), also from eBioscience (Supplementary Fig. 4). Foxp3 staining for cells from knockout mice was performed with the Foxp3 staining kit by eBioscience (00-5523-00) in accordance with their 'One-step protocol for intracellular (nuclear) proteins'. Data were collected using either a FACS Calibur or LSR II (Both BD Biosciences), then analysed using Flow Jo software (Treestar)[49,50].

Quantification of cytokine secretion using ELISA. Naive T cells from knockout mice and their wild-type controls were cultured as described above, their supernatants were collected after 72 h, and cytokine concentrations were determined by ELISA (antibodies for IL-17 and IL-10 from BD Bioscience) or by cytometric bead array for the indicated cytokines (BD Bioscience), according to the manufacturers' instructions (Fig. 5 and Supplementary Fig. 11).

Microarray data. Naive T cells were isolated from wild-type mice, and treated with IL-6 and TGF-β1. Affymetrix microarrays HT_MG-430A were used to measure the resulting mRNA levels at 18 different time points (0.5–72 h; Fig. 1b). Cells treated initially with IL-6, TGF-β1 and with addition of IL-23 after 48 h were profiled at four time points (50–72 h). As control, we used time- and culture-matched wild-type naive T cells stimulated under T_H0 conditions. Biological replicates were measured in 8 of the 18 time points (1 h, 4 h, 10 h, 20 h, 30 h, 42 h, 52 h, 60 h) with high reproducibility ($r^2 > 0.98$). For further validation we compared the differentiation time course to published microarray data of T_H17 cells and naive T cells[51] (Supplementary Fig. 1c). In an additional data set, naive T cells were isolated from wild-type and *Il23r*$^{-/-}$ mice, and treated with IL-6, TGF-β1 and IL-23 and profiled at four different time points (49 h, 54 h, 65 h, 72 h). Expression data were pre-processed using the RMA algorithm followed by quantile normalization[52].

Detecting differentially expressed genes. Differentially expressed genes (comparing to the T_H0 control) were found using four methods: (1) Fold change. Requiring a twofold change (up or down) during at least two time points. (2) Polynomial fit. We used the EDGE software[53,54], designed to identify differential expression in time course data, with a threshold of q-value ≤ 0.01. (3) Sigmoidal fit. We used an algorithm similar to EDGE while replacing the polynomials with a sigmoid function, which is often more adequate for modelling time course gene expression data[55]. We used a threshold of q-value ≤ 0.01. (4) ANOVA. Gene expression is modelled by: time (using only time points for which we have more than one replicate) and treatment ('TGF-β1 + IL-6' or 'T_H0'). The model takes into account each variable independently, as well as their interaction. We report cases in which the P value assigned with the treatment parameter or the interaction parameter passed an FDR threshold of 0.01.

Overall, we saw substantial overlap between the methods (average of 82% between any pair of methods). We define the differential expression score of a gene as the number of tests that detected it. As differentially expressed genes, we report cases with differential expression score >2.

For the *Il23r*$^{-/-}$ time course (compared to the wild-type T cells) we used methods (1)–(3) (above). Here we used a fold change cutoff of 1.5, and report genes detected by at least two tests.

Clustering. We considered several ways for grouping the differentially expressed genes, based on their time course expression data: (1) for each time point, we defined two groups ((a) all the genes that are overexpressed, and (b) all the genes that are under-expressed relative to T_H0 cells (see below)); (2) for each time point, we defined two groups ((a) all the genes that are induced, and (b) all the genes that are repressed, comparing to the previous time point); (3) k-means clustering using only the T_H17 polarizing conditions. We used the minimal k, such that the within-cluster similarity (average Pearson correlation with the cluster's centroid) was higher than 0.75 for all clusters; and, (4) k-means clustering using a concatenation of the T_H0 and T_H17 profiles.

For methods (1) and (2), to decide whether to include a gene, we considered its original mRNA expression profiles (T_H0, T_H17) and their approximations as sigmoidal functions[55] (thus filtering transient fluctuations). We require that the fold change levels (compared to T_H0 (method 1) or to the previous time point (method 2)) pass a cutoff defined as the minimum of the following three values: (1) 1.7; (2) mean + s.d. of the histogram of fold changes across all time points; or (3) the maximum fold change across all time points. The clusters presented in Fig. 1b were obtained with method (4). The groupings from methods (1), (2) and (4) are provided in Supplementary Table 2.

Regulatory network inference. We identified potential regulators of T_H17 differentiation by computing overlaps between their putative targets and sets of differentially expressed genes grouped according to methods (1)–(4) above. We assembled regulator–target associations from several sources: (1) *in vivo* DNA binding profiles (typically measured in other cells) of 298 transcriptional regulators[12–17]; (2) transcriptional responses to the knockout of 11 regulatory proteins[6,43,49,56–60]; (3) additional potential interactions obtained by applying the Ontogenet algorithm (V. Jojic *et al.*, submitted; regulatory model available at: http://www.immgen.org/ModsRegs/modules.html) to data from the mouse ImmGen consortium (http://www.immgen.org; January 2010 release[19]), which includes 484 microarray samples from 159 cell subsets from the innate and adaptive immune system of mice; (4) a statistical analysis of *cis*-regulatory element enrichment in promoter regions[18]; and (5) the transcription factor enrichment module of the IPA software (http://www.ingenuity.com/). For every transcription factor in our database, we computed the statistical significance of the overlap between its putative targets and each of the groups defined above using a Fisher's exact test. We include cases where $P < 5 \times 10^{-5}$ and the fold enrichment >1.5.

Each edge in the regulatory network was assigned a time stamp based on the expression profiles of its respective regulator and target nodes. For the target node, we considered the time points at which a gene was either differentially expressed or significantly induced or repressed with respect to the previous time point (similarly to grouping methods (1) and (2) above). We defined a regulator node as 'absent' at a given time point if: (i) it was under expressed compared to T_H0; or (ii) the expression is low (<20% of the maximum value in time) and the gene was not overexpressed compared to T_H0; or, (iii) up to this point in time the gene was not expressed above a minimal expression value of 100. As an additional constraint, we estimated protein expression levels using the model from ref. 20 and using a sigmoidal fit[55] for a continuous representation of the temporal expression profiles, and the ProtParam software[61] for estimating protein half-lives. We require that, in a given time point, the predicted protein level be no less than 1.7-fold below the maximum value attained during the time course, and not be less than 1.7-fold below the T_H0 levels. The timing assigned to edges inferred based on a time-point-specific grouping (grouping methods (1) and (2) above) was limited to that specific time point. For instance, if an edge was inferred based on enrichment in the set of genes induced at 1 h (grouping method (2)), it will be assigned a '1 h' time stamp. This same edge could then only have additional time stamps if it was revealed by additional tests.

Selection of nanostring signature genes. The selection of the 275-gene signature (Supplementary Tables 5 and 6) combined several criteria to reflect as many aspects of the differentiation program as was possible. We defined the following requirements: (1) the signature must include all of the transcription factors that belong to a T_H17 microarray signature (comparing to other CD4^{+} T cells[51], see

Supplementary Methods); that are included as regulators in the network and have a differential expression score >1; or that are strongly differentially expressed (differential expression score = 4); (2) it must include at least 10 representatives from each cluster of genes that have similar expression profiles (using clustering method (4) above); (3) it must contain at least 5 representatives from the predicted targets of each transcription factor in the different networks; (4) it must include a minimal number of representatives from each enriched Gene Ontology (GO) category (computed across all differentially expressed genes); and (5) it must include a manually assembled list of ~100 genes that are related to the differentiation process, including the differentially expressed cytokines, cytokine receptors and other cell surface molecules. Because these different criteria might generate substantial overlaps, we used a set-cover algorithm to find the smallest subset of genes that satisfies all of five conditions. We added to this list 18 genes whose expression showed no change (in time or between treatments) in the microarray data.

The 86-gene signature (used for the Fluidigm BioMark qPCR assay) is a subset of the 275-gene signature, selected to include all the key regulators and cytokines discussed. We added to this list 10 control genes (Supplementary Table 5).

Selection of perturbation targets. We used an unbiased approach to rank candidate regulators—transcription factor or chromatin modifier genes—of T_H17 differentiation. Our ranking was based on the following features: (a) whether the gene encoding the regulator belonged to the T_H17 microarray signature (comparing to other $CD4^+$ T cells[51], see Supplementary Methods); (b) whether the regulator was predicted to target key T_H17 molecules (IL-17, lL-21, IL-23r and ROR-γt); (c) whether the regulator was detected based on both perturbation and physical binding data from the IPA software (http://www.ingenuity.com/); (d) whether the regulator was included in the network using a cutoff of at least 10 target genes; (e) whether the gene coding for the regulator was significantly induced in the T_H17 time course—we only consider cases where the induction happened after 4 h to exclude nonspecific hits; (f) whether the gene encoding the regulator was differentially expressed in response to T_H17-related perturbations in previous studies. For this criterion, we assembled a database of transcriptional effects in perturbed T_H17 cells, including: knockouts of *Batf* (ref. 56), *Rorc* (S. Xiao *et al.*, unpublished), *Hif1a* (ref. 57), *Stat3* and *Stat5* (refs 43, 62), *Tbx21* (A. Awasthi *et al.*, unpublished), *Il23r* (this study), and *Ahr* (ref. 59). We also included data from the T_H17 response to digoxin[63] and halofuginone[64], as well as information on direct binding by ROR-γt as inferred from ChIP-seq data (S. Xiao *et al.*, unpublished). For each regulator, we counted the number of conditions in which it came up as a significant hit (up/downregulated or bound); for regulators with 2 to 3 hits (quantiles 3 to 7 out of 10 bins), we then assigned a score of 1; for regulators with more than 3 hits (quantiles 8–10), we assigned a score of 2 (a score of 0 is assigned otherwise); and, (g) the differential expression score of the gene in the T_H17 time course.

We ordered the regulators lexicographically by the above features according to the order: (a), (b), (c), (d), (sum of (e) and (f)), (g); that is, first sort according to (a) then break ties according to (b), and so on. We exclude genes that are not over-expressed during at least one time point. As an exception, we retained predicted regulators (features (c) and (d)) that had additional external validation (feature (f)). To validate this ranking, we used a supervised test: we manually annotated 72 regulators that were previously associated with T_H17 differentiation. All of the features are highly specific for these regulators ($P < 10^{-3}$). Moreover, using a supervised learning method (Naive Bayes), the features provided good predictive ability for the annotated regulators (accuracy of 71%, using fivefold cross validation), and the resulting ranking was highly correlated with our unsupervised lexicographic ordering (Spearman correlation >0.86).

We adapted this strategy for ranking protein receptors. To this end, we excluded feature (c) and replaced the remaining 'protein-level' features ((b) and (d)) with the following definitions: (b) whether the respective ligand is induced during the T_H17 time course; and, (d) whether the receptor was included as a target in the network using a cutoff of at least 5 targeting transcriptional regulators.

Gene knockdown using silicon nanowires. 4 × 4 mm silicon nanowire substrates were prepared and coated with 3 µl of a 50 µM pool of four siGENOME siRNAs (Dharmcon) in 96-well tissue culture plates, as previously described[10]. Briefly, 150,000 naive T cells were seeded on siRNA-laced nanowires in 10 µl of complete media and placed in a cell culture incubator (37 °C, 5% CO_2) to settle for 45 min before full media addition. These samples were left undisturbed for 24 h to allow target transcript knockdown. Afterward, siRNA-transfected T cells were activated with anti-CD3/CD28 dynabeads (Invitrogen), according to the manufacturer's recommendations, under T_H17 polarization conditions (TGF-β1 and IL-6, as above). 10 or 48 h post-activation, culture media was removed from each well and samples were gently washed with 100 µl of PBS before being lysed in 20 µl of buffer TCL (Qiagen) supplemented with 2-mercaptoethanol (1:100 by volume). After mRNA was collected in Turbocapture plates (Qiagen) and converted to cDNA using Sensiscript RT enzyme (Qiagen), qRT–PCR was used to validate both knockdown levels and phenotypic changes relative to 8–12 non-targeting siRNA control samples, as previously described[65]. A 60% reduction in target mRNA was used as the knockdown threshold. In each knockdown experiment, each individual siRNA pool was run in quadruplicate; each siRNA was tested in at least three separate experiments (Supplementary Fig. 9).

mRNA measurements in perturbation assays. We used the nCounter system, presented in full in ref. 66, to measure a custom CodeSet constructed to detect a total of 293 genes, selected as described above. We also used the Fluidigm BioMark HD system to measure a smaller set of 96 genes. Finally, we used RNA-seq to follow up and validate 12 of the perturbations. Details of the experimental and analytical procedures of these analyses are provided in the Supplementary Methods.

Profiling Tsc22d3 DNA binding using ChIP-seq. ChIP-seq for Tsc22d3 was performed as previously described[67] using an antibody from Abcam. The analysis of this data was performed as previously described[7] and is detailed in the Supplementary Methods.

Estimating statistical significance of monochromatic interactions between modules. The functional network in Fig. 4b consists of two modules: positive and negative. We compute two indices: (1) within-module index: the percentage of positive edges between members of the same module (that is, downregulation in knockdown/knockout); and (2) between-module index: the percentage of negative edges between members of different modules. We shuffled the network 1,000 times, while maintaining the nodes' out degrees (that is, number of outgoing edges) and edges' signs (positive/ negative), and re-computed the two indices. The reported *P* values were computed using a *t*-test.

46. Kim, U. *et al.* The B-cell-specific transcription coactivator OCA-B/OBF-1/Bob-1 is essential for normal production of immunoglobulin isotypes. *Nature* **383,** 542–547 (1996).
47. Wang, V. E., Tantin, D., Chen, J. & Sharp, P. A. B cell development and immunoglobulin transcription in Oct-1-deficient mice. *Proc. Natl Acad. Sci. USA* **101,** 2005–2010 (2004).
48. Bettelli, E. *et al.* Reciprocal developmental pathways for the generation of pathogenic effector T_H17 and regulatory T cells. *Nature* **441,** 235–238 (2006).
49. Awasthi, A. *et al.* A dominant function for interleukin 27 in generating interleukin 10-producing anti-inflammatory T cells. *Nature Immunol.* **8,** 1380–1389 (2007).
50. Awasthi, A. *et al.* Cutting edge: IL-23 receptor gfp reporter mice reveal distinct populations of IL-17-producing cells. *J. Immunol.* **182,** 5904–5908 (2009).
51. Wei, G. *et al.* Global mapping of H3K4me3 and H3K27me3 reveals specificity and plasticity in lineage fate determination of differentiating $CD4^+$ T cells. *Immunity* **30,** 155–167 (2009).
52. Reich, M. *et al.* GenePattern 2.0. *Nature Genet.* **38,** 500–501 (2006).
53. Storey, J., Xiao, W., Leek, J., Tompkins, R. & Davis, R. Significance analysis of time course microarray experiments. *Proc. Natl Acad. Sci. USA* **102,** 12837–12482 (2005).
54. Leek, J. T., Monsen, E., Dabney, A. R. & Storey, J. D. EDGE: extraction and analysis of differential gene expression. *Bioinformatics* **22,** 507–508 (2006).
55. Chechik, G. & Koller, D. Timing of gene expression responses to environmental changes. *J. Comput. Biol.* **16,** 279–290 (2009).
56. Schraml, B. U. *et al.* The AP-1 transcription factor Batf controls T_H17 differentiation. *Nature* **460,** 405–409 (2009).
57. Shi, L. Z. *et al.* HIF1α-dependent glycolytic pathway orchestrates a metabolic checkpoint for the differentiation of T_H17 and T_{reg} cells. *J. Exp. Med.* **208,** 1367–1376 (2011).
58. Durant, L. *et al.* Diverse targets of the transcription factor STAT3 contribute to T cell pathogenicity and homeostasis. *Immunity* **32,** 605–615 (2010).
59. Jux, B., Kadow, S. & Esser, C. Langerhans cell maturation and contact hypersensitivity are impaired in aryl hydrocarbon receptor-null mice. *J. Immunol.* **182,** 6709–6717 (2009).
60. Xiao, S. *et al.* Retinoic acid increases $Foxp3^+$ regulatory T cells and inhibits development of Th17 cells by enhancing TGF-β-driven Smad3 signaling and inhibiting IL-6 and IL-23 receptor expression. *J. Immunol.* **181,** 2277–2284 (2008).
61. Wilkins, M. R. *et al.* Protein identification and analysis tools in the ExPASy server. *Methods Mol. Biol.* **112,** 531–552 (1999).
62. Durant, L. *et al.* Diverse targets of the transcription factor STAT3 contribute to T cell pathogenicity and homeostasis. *Immunity* **32,** 605–615 (2010).
63. Huh, J. R. *et al.* Digoxin and its derivatives suppress T_H17 cell differentiation by antagonizing RORγt activity. *Nature* **472,** 486–490 (2011).
64. Sundrud, M. S. *et al.* Halofuginone inhibits T_H17 cell differentiation by activating the amino acid starvation response. *Science* **324,** 1334–1338 (2009).
65. Chevrier, N. *et al.* Systematic discovery of TLR signaling components delineates viral-sensing circuits. *Cell* **147,** 853–867 (2011).
66. Geiss, G. K. *et al.* Direct multiplexed measurement of gene expression with color-coded probe pairs. *Nature Biotechnol.* **26,** 317–325 (2008).
67. Ram, O. *et al.* Combinatorial patterning of chromatin regulators uncovered by genome-wide location analysis in human cells. *Cell* **147,** 1628–1639 (2011).